How to cite: *Angew. Chem. Int. Ed.* **2021**, *60*, 17735–17743
International Edition: doi.org/10.1002/anie.202107264
German Edition: doi.org/10.1002/ange.202107264

CO_2 Utilization

Visualizing Element Migration over Bifunctional Metal-Zeolite Catalysts and its Impact on Catalysis

Yuhao Wang[+], Genyuan Wang[+], Lars I. van der Wal, Kang Cheng, Qinghong Zhang, Krijn P. de Jong,* and Ye Wang**

Dedicated to the 100th anniversary of Xiamen University

Abstract: *The catalytic performance of composite catalysts is not only affected by the physicochemical properties of each component, but also the proximity and interaction between them. Herein, we employ four representative oxides (In_2O_3, ZnO, Cr_2O_3, and ZrO_2) to combine with H-ZSM-5 for the hydrogenation of CO_2 to hydrocarbons directed by methanol intermediate and clarify the correlation between metal migration and the catalytic performance. The migration of metals to zeolite driven by the harsh reaction conditions can be visualized by electron microscopy, meanwhile, the change of zeolite acidity is also carefully characterized. The protonic sites of H-ZSM-5 are neutralized by mobile indium and zinc species via a solid ion-exchange mechanism, resulting in a drastic decrease of C_{2+} hydrocarbon products over In_2O_3/H-ZSM-5 and ZnO/H-ZSM-5. While, the thermomigration ability of chromium and zirconium species is not significant, endowing Cr_2O_3/H-ZSM-5 and ZrO_2/H-ZSM-5 catalysts with high selectivity of C_{2+} hydrocarbons.*

Introduction

Bifunctional catalysts composed of metal (oxide) and zeolites have been widely applied in key catalytic processes, such as biomass upgrading, oil refining, and hydrogenation of CO/CO_2 to hydrocarbons.[1] The tandem catalysis realized by bifunctional catalysts not only integrates different reactions but also enhances the catalytic performances by the so-called synergistic effect.[2] Very recently several groups reported the successful combination of the production of methanol from CO/CO_2 with the further transformation of methanol into lower olefins and aromatics, achieved by oxide-zeolite catalysts.[3] These studies have triggered the research on the direct hydrogenation of CO/CO_2 to hydrocarbon fuels and chemicals.[4] Different from the conventional Fischer–Tropsch (FT) synthesis, which only offers a broad product distribution due to the polymerization mechanism, the C-C coupling over bifunctional catalysts is conducted inside the zeolite channels or cages, thus enabling the controllable synthesis of desired products.[5] Besides, the formation of hydrocarbons can thermodynamically drive the conversion of CO/CO_2, providing comparable conversion levels as FT synthesis.[1c,3b,4b,6] Despite the numerous advantages described, the side effects of the emerging bifunctional systems were rarely mentioned and investigated.

In principle, the active catalytic phase normally possesses a large surface area and defective structure of high surface energy, which is easy to become stable but inactive phases.[7] Although the presence of high-pressure hydrogen has been confirmed to be beneficial to the stability of bifunctional systems because the formation of polycyclic aromatic species on zeolites could be suppressed,[8] most of the reported bifunctional catalysts more or less suffer from slow deactivation.[6,9] As briefly summarized in Scheme 1, the cause of deactivation for bifunctional catalysts may be related to the coking of zeolite due to the hydrocarbon pool mechanism for the conversion of methanol to hydrocarbons (MTH) reaction and the sintering/reconstruction of the metal nanoparticles (NPs) induced by harsh reaction conditions.[10] Additionally, in bifunctional systems, the migration of metal species to zeolite driven by high temperature, reductive atmosphere, and the formation of water vapor is also a great concern.[11] The consequences of metal migration may include but not be

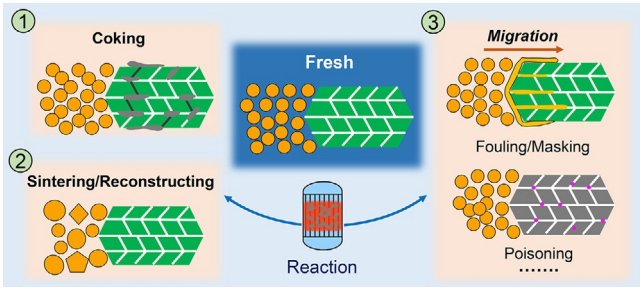

Scheme 1. Major types of deactivation mechanism in bifunctional catalysis.

[*] Dr. Y. Wang,[+] G. Wang,[+] Dr. K. Cheng, Prof. Q. Zhang, Prof. Y. Wang
State Key Laboratory of Physical Chemistry of Solid Surfaces, Collaborative Innovation Center of Chemistry for Energy Materials, National Engineering Laboratory for Green Chemical Productions of Alcohols, Ethers and Esters, College of Chemistry and Chemical Engineering, Xiamen University
Xiamen 361005 (China)
E-mail: kangcheng@xmu.edu.cn
wangye@xmu.edu.cn
L. I. van der Wal, Prof. K. P. de Jong
Inorganic Chemistry and Catalysis, Debye Institute for Nanomaterials Science, Utrecht University
3584 CG Utrecht (The Netherlands)
E-mail: k.p.dejong@uu.nl
[+] These authors contributed equally to this work.
Supporting information and the ORCID identification number(s) for the author(s) of this article can be found under: https://doi.org/10.1002/anie.202107264.

limited to the fouling, masking, and poisoning of the active sites on zeolites (Scheme 1). It is noteworthy that these phenomena often take place simultaneously.

As early as the 1970s, some researchers reported the solid-state reaction between H-type zeolites and metal salts.[12] Several mechanisms have been proposed, including (1) contact-induced solid-state reaction, (2) gas-phase mediated processes, (3) oxidative and reductive solid-state reaction, and (4) Water-induced solid-state reaction.[13] Some explained the migration of metal species to the support with a large surface area by the "Spontaneous Monolayer Dispersion".[14] In many cases, the migration of metal ions neutralizes the Brønsted acid sites (BAS) of zeolites and leads to the formation of inactive silicates or aluminates, causing deactivation in the direct hydrogenation of CO/CO_2 to hydrocarbon products.[4a,15] Besides, the mobile metal species may reassemble into metal clusters or NPs during reaction, which may block and cover the micropore channels of zeolites.[4a] Whereas, the replacement of protonic sites of zeolites by the metal ions is sometimes employed to promote the reaction.[16] For instance, it was reported that molybdenum ions placed in the micropore channels of H-ZSM-5 served as the active center for methane aromatization.[17] The incorporation of zinc into H-ZSM-5 could also promote the MTH reaction, attributing to the contact synergy between the oxides and the zeolites.[18] Overall, the influence of metal migration on bifunctional catalysts is quite complicated, especially for the multicomponent systems operating under harsh reaction conditions. Up to now, few studies have touched upon the impact of metal migration from oxides to zeolites on the catalytic behaviors of bifunctional catalysts in C1 chemistry.

In this work, four frequently used oxides,[4c,19] i.e., In_2O_3, ZnO, Cr_2O_3, and ZrO_2, have been selected as the methanol synthesis function to integrate with H-ZSM-5 by a simple physical mixing method. We attempt to visualize the migration process of metal components over bifunctional catalysts in the selective hydrogenation of CO_2 and reveal its correlation with zeolite acidity and catalyst decay. The bifunctional catalysts before and after CO_2 hydrogenation under industrially relevant conditions were carefully characterized through transmission electron microscopy and a series of spectroscopic characterizations. The interplay between metal migration and catalytic performances will be particularly described.

Results and Discussion

Catalytic Performances of CO_2 Hydrogenation

In this work, a commercial H-ZSM-5 with an atomic Si/Al ratio of 15 was employed to catalyze the MTH reaction. H-ZSM-5 with MFI topology is the most representative zeolite to catalyze the formation of hydrocarbon liquids in C1 chemistry.[20] Besides, it is well known that the catalytic activity and product selectivity are closely related to the selection of oxides and the integration manners of the active functional components over bifunctional catalysts.[21] The choice of metal oxides for CO_2 activation is quite exquisite, among which In_2O_3, ZnO, Cr_2O_3, ZrO_2, and their binary/ternary composites have been frequently employed. The representative four pristine oxides exhibited different CO_2 conversion levels at 350 °C, decreasing in the order of $In_2O_3 > ZnO > Cr_2O_3 > ZrO_2$ (Table S1). Besides methanol, the high reaction temperature induced the formation of CO by the reverse water-gas shift (RWGS) reaction. The integration of oxide in the upper bed and H-ZSM-5 in the lower bed could convert all the methanol intermediates into hydrocarbon products (Figure S1 and Table S1), indicating the acid density of H-ZSM-5 was sufficient to conduct MTH function. However, the dual-bed mode is not preferential in bifunctional catalysis because it cannot provide sufficient proximity between different active sites for efficient synergy.[21c,22] In the following study, a commonly used method of physical mixing was used to combine oxide and H-ZSM-5.

As shown in Figure 1a, the major product over bifunctional In_2O_3/H-ZSM-5 was methanol and dimethyl ether (DME) in CO_2 hydrogenation, instead of C_{2+} hydrocarbons. The Brønsted acid sites are generally considered as the active sites for catalyzing C-C coupling.[23] Therefore, it can be inferred that the acidity of H-ZSM-5 was strongly poisoned by the close integration with In_2O_3. Likewise, the formation of methanol and DME was observed over ZnO/H-ZSM-5, but a considerable amount of C_{2+} hydrocarbons (ca. 55%) was also formed (Figure 1b). While for both Cr_2O_3/H-ZSM-5 and ZrO_2/H-ZSM-5 (Figures 1c,d), the major product was C_{2+} hydrocarbons together with methane, without the formation of methanol. The choice of oxide component with moderate hydrogenation ability is important to get high selectivity of C_{2+} hydrocarbons, while the use of typical Cu-ZnO as methanol synthesis component for bifunctional catalysts favored the formation of methanol, DME, and C_2–C_4 paraffins (Table S1). Catalyst stability is an important performance descriptor for bifunctional catalysts. The activity and product distribution became relatively stable after 30 h on stream, indicating that the catalyst evolution mainly occurred at the initial stage of the reaction (Figure S2). Overall, these findings suggest that the combination with oxides possibly affected the acidity of zeolite or the accessibility of acid sites to the intermediates, and the degree of influence on catalytic performance was strongly dependent on the type of oxide.

The Migration of Indium

To visualize the element migration, HAADF-STEM imaging and the corresponding EDX mapping analysis were conducted to disclose the changes of catalysts during reaction over the fresh and used bifunctional In_2O_3/H-ZSM-5 catalysts. It was observed that the aggregates of In_2O_3 NPs were closely attached to the outer surface of H-ZSM-5 crystals over the fresh catalyst (Figures 2a–d), providing a close distance between oxides and H-ZSM-5. After CO_2 hydrogenation, a drastic morphological change of indium species was visualized, while the shape of H-ZSM-5 was still sustained (Figures 2e–h). First, the indium NPs sintered severely into larger ones near H-ZSM-5 crystals. Second, indium NPs were found to be redispersed on H-ZSM-5, and enriched along the

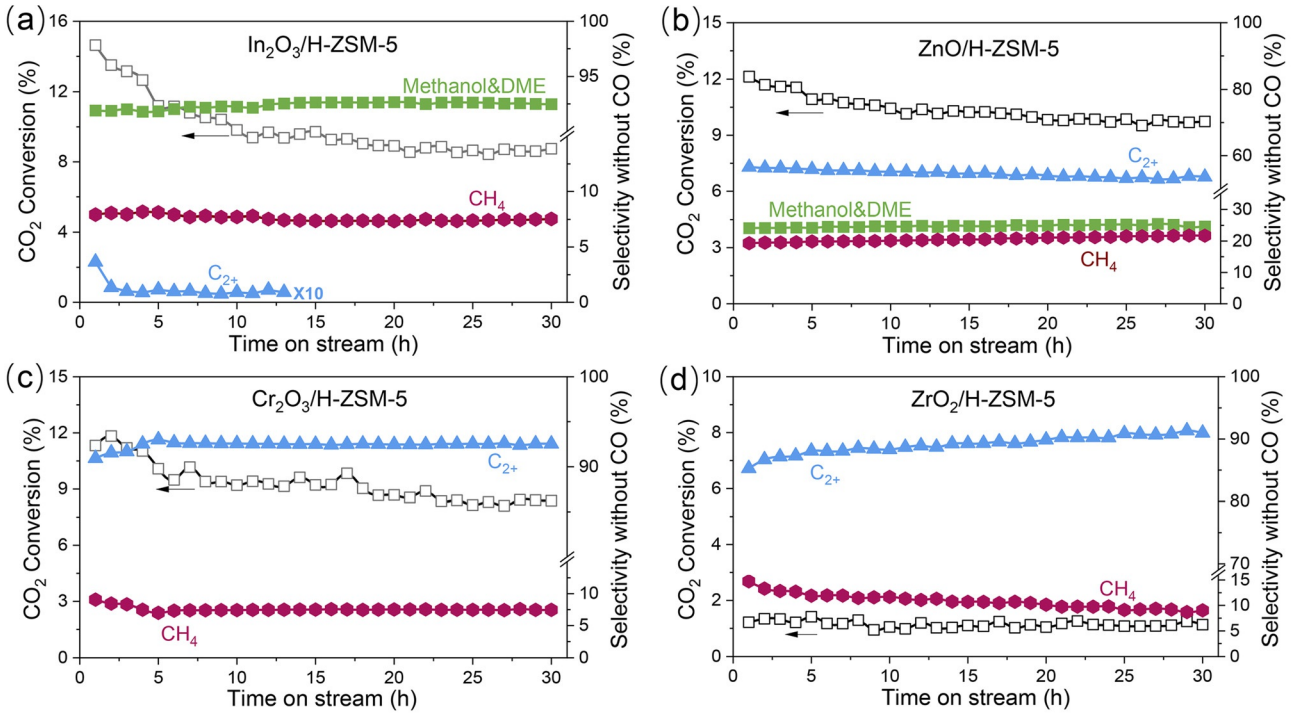

Figure 1. CO_2 conversion and product selectivity excluding CO over different bifunctional catalysts. a) In_2O_3/H-ZSM-5, b) ZnO/H-ZSM-5, c) Cr_2O_3/H-ZSM-5, d) ZrO_2/H-ZSM-5. Reaction condition: $H_2/CO_2 = 3{:}1$, oxide/H-ZSM-5 mass ratio = 1:1, $W_{cat} = 0.3$ g, time on stream 30 h, $T = 350\,°C$, $P = 3$ MPa, $F = 30$ mL min^{-1}. Detailed catalytic performances are displayed in Table S1.

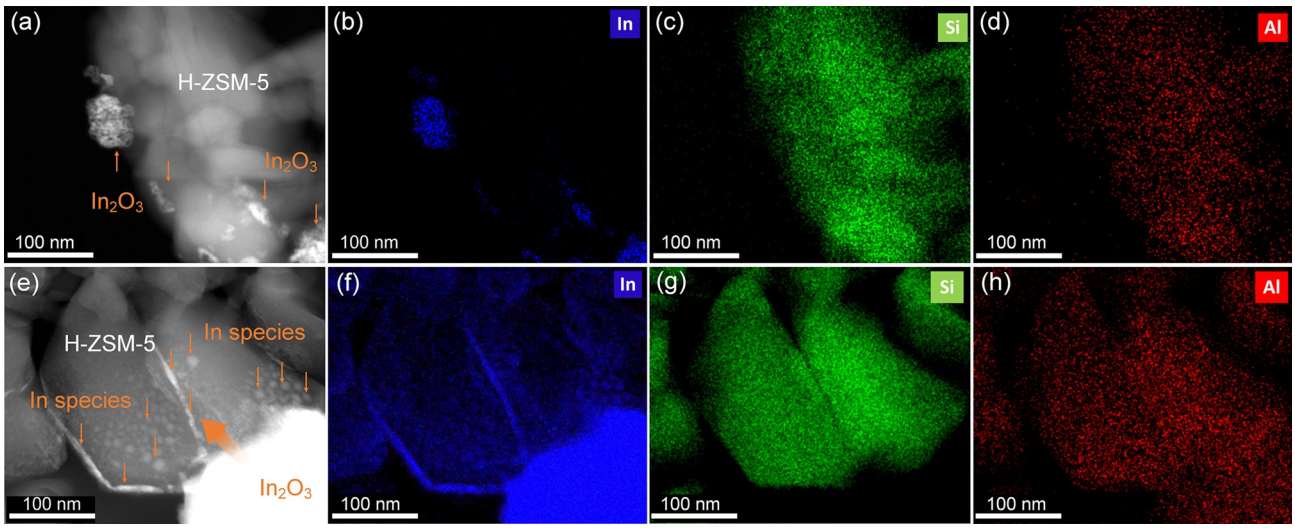

Figure 2. HAADF-STEM images and corresponding element mapping of a)–d) fresh In_2O_3/H-ZSM-5 and e)–h) used In_2O_3/H-ZSM-5.

edges of the H-ZSM-5, indicating the strong mobility of indium species under reaction conditions. The evolution of catalyst structures of In_2O_3/H-ZSM-5 was also revealed by XRD that the diffraction peaks for In_2O_3 became stronger and sharper (Figure S3a). Overall, the H-ZSM-5 component was contaminated and covered by indium species. It is noteworthy that smaller indium species, such as indium ions and clusters, cannot be observed by HAADF-STEM imaging.

To further investigate the metal migration mechanism and its impact on the properties of the composite catalysts, we characterized a series of catalysts prepared by different methods or pretreated by different conditions (See the details in Supporting Information). The X-ray photoelectron spectroscopy (XPS) spectra of the pristine In_2O_3 exhibited two signals with binding energy (BE) values at approximately 451.7 eV (In $3d_{5/2}$) and 444.2 eV (In $3d_{3/2}$), respectively (Figure 3a). The In_2O_3/H-ZSM-5-*I* prepared by an impregnation method was analyzed as a reference for indium ions being located on the protonic sites of the H-ZSM-5. The In_2O_3/H-ZSM-5-*I* showed higher energy with a 1.3 eV increment comparing with that of In_2O_3. This could be ascribed to the strong interaction between indium species and zeolites,

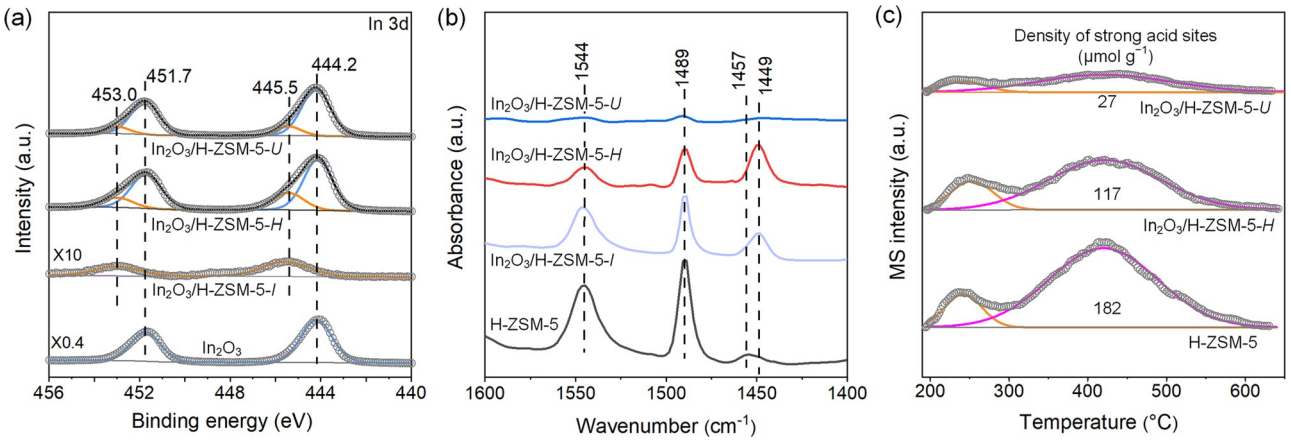

Figure 3. The spectra of a) XPS for In_2O_3, In_2O_3/H-ZSM-5-*I*, In_2O_3/ZSM-5-*H* and In_2O_3/H-ZSM-5-*U*, b) pyridine-adsorption FTIR for H-ZSM-5, In_2O_3/H-ZSM-5-*I*, In_2O_3/ZSM-5-*H* and In_2O_3/H-ZSM-5-*U*, c) NH_3-TPD for H-ZSM-5, In_2O_3/ZSM-5-*H* and In_2O_3/H-ZSM-5-*U*. The acid density was normalized to the weight of H-ZSM-5.

causing the electron transfer from indium to H-ZSM-5.[11b,24] The XPS spectra of In_2O_3/H-ZSM-5-*H* treated in the argon flow at 400 °C were similar to that of In_2O_3. However, two shoulder peaks appeared at 453.0 and 445.5 eV, indicating the formation of the indium species that had a strong interaction with H-ZSM-5. Therefore, even the heat treatment could induce the migration of indium species to zeolite. For the used In_2O_3/H-ZSM-5-*U* catalyst, the shoulder peaks could also be detected, suggesting the indium species were present within zeolites after CO_2 hydrogenation.

Pyridine-adsorbed FTIR (Py-FTIR) was used to identify Brønsted and Lewis acid sites (LAS) on catalysts (Figure 3b). The bands at 1544 cm^{-1}, 1457 cm^{-1}, and 1489 cm^{-1} can be assigned to the BAS, LAS, and the combination of the two, respectively.[25] Compared with pristine H-ZSM-5, the band of BAS decreased with the increase of an additional band at 1449 cm^{-1} on In_2O_3/H-ZSM-5-*I* (Figure 3b). It was reported that the adsorption of pyridine on some monovalent metal cations (a type of LAS), such as Na^+, led to the appearance of a band slightly below 1450 cm^{-1}.[26] Thus, the evolution of acidity over In_2O_3/H-ZSM-5 could be attributed to the exchange of the monovalent indium species with the protonic sites of H-ZSM-5.[27] After the reaction, the IR bands of both BAS and LAS almost disappeared over In_2O_3/H-ZSM-5-*U*. In_2O_3 can be reduced to its metallic phase (Figure S4), which liquefy at relatively low temperatures (melting point 156 °C). Therefore, we can speculate that indium species in the form of cations or liquid metal could poison or cover the acid sites of H-ZSM-5 by fast migration during reaction (Figure S5).

The NH_3-TPD profiles of H-ZSM-5 exhibit a typical bimodal characteristic of zeolite with MFI structure (Figure 3c).[28] The peak desorbed at a temperature above 300 °C is generally ascribed to the ammonia adsorbed on the strong acid sites, probably the acidic hydroxyl (Si-OH-Al) groups, and can be used to quantify the change of BAS density.[28,29] The peak below 300 °C is probably caused by the desorption of ammonia of the physical adsorption, weak adsorption by LAS, and hydrogen bonding.[30] The desorption peaks of ammonia decreased dramatically over In_2O_3/H-ZSM-5-*H* and In_2O_3/H-ZSM-5-*U*, implying that the acid sites were neutralized by indium cations or covered by metallic indium.

The Migration of Zinc

The HAADF-STEM images of the fresh ZnO/H-ZSM-5 reveal that both ZnO particles and H-ZSM-5 crystals were intact without observable metal migration (Figures 4a,b and S6). The average size of ZnO particles was around 50 nm.

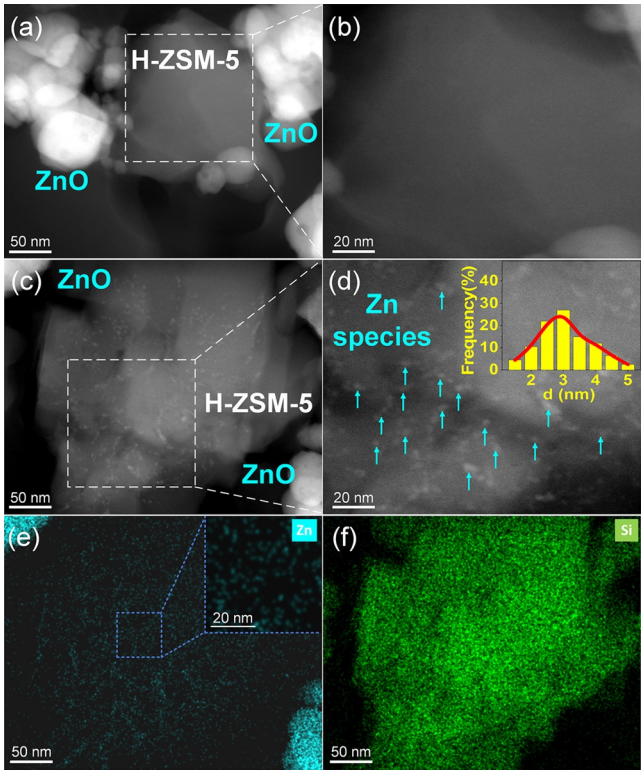

Figure 4. HAADF-STEM images of a),b) fresh ZnO/H-ZSM-5 and c)–f) used ZnO/H-ZSM-5. The inset in (d) shows the size distribution of zinc species.

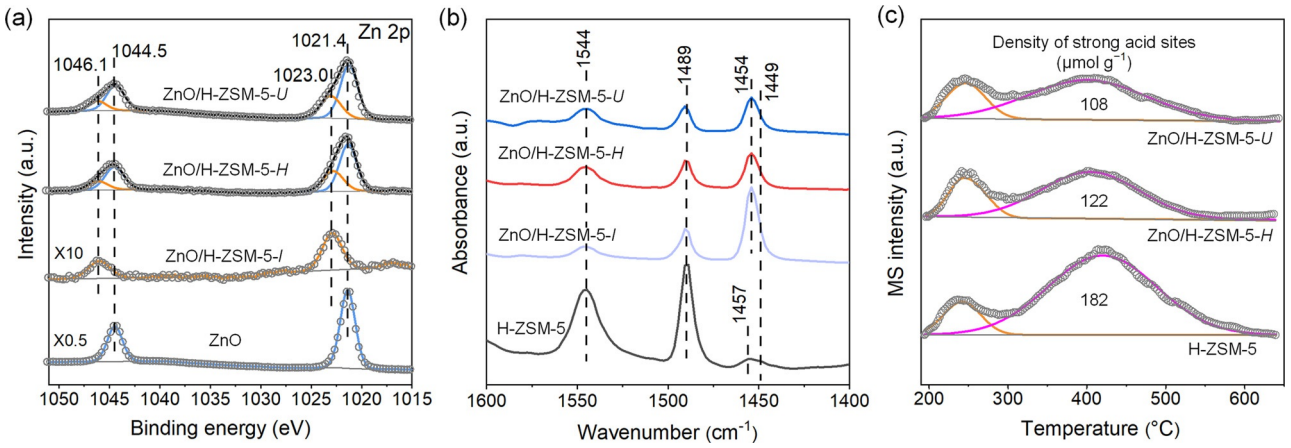

Figure 5. The spectra of a) XPS for ZnO, ZnO/H-ZSM-5-*I*, ZnO/ZSM-5-*H* and ZnO/H-ZSM-5-*U*, b) pyridine-adsorption FTIR for H-ZSM-5, ZnO/H-ZSM-5-*I*, ZnO/ZSM-5-*H* and ZnO/H-ZSM-5-*U*, c) NH_3-TPD for H-ZSM-5, ZnO/ZSM-5-*H* and ZnO/H-ZSM-5-*U*. The acid density was normalized to the weight of H-ZSM-5.

However, after reaction, the surface of H-ZSM-5 was covered by small dispersed zinc particles (2–3 nm), together with the existence of large ZnO particles (Figures 4c–f), indicating the strong mobility of zinc under reductive atmosphere. While the crystal structures of H-ZSM-5 did not change significantly (Figure S3b).

Compared with pristine ZnO, the BE values for Zn 2p of ZnO/H-ZSM-5-*I* shifted to high values, indicating the zinc species on protonic sites of H-ZSM-5 were strongly stabilized (Figure 5a). For ZnO/H-ZSM-5-*H* and ZnO/H-ZSM-5-*U*, the apparent shoulder bands located at high BE values revealed that the zinc species could migrate to zeolites driven by heat treatment or CO_2 hydrogenation, like In-based bifunctional catalysts. The proportion of shoulder peaks was similar for ZnO/H-ZSM-5-*H* and ZnO/H-ZSM-5-*U* (Table S2). The Py-FTIR suggested that the majority of the acidity over ZnO/H-ZSM-5-*I* was LAS, instead of BAS (Figure 5b). The additional band at 1454 cm^{-1} was lower than 1457 cm^{-1} caused by pyridine adsorption on Al^{3+} cations,[31] but higher than 1449 cm^{-1} caused by pyridine adsorption on monovalent metal cations. Thus, the zinc species on protonic sites of H-ZSM-5 were probably bivalent. Several groups claimed that the $[ZnOH]^+$ species were the main ingredient located in the protonic sites of the zeolites.[18] To further confirm the existence of $[ZnOH]^+$ species, the IR characterization for O-H vibration of the ZnO, H-ZSM-5, and ZnO/H-ZSM-5 samples prepared or treated by different methods were performed (Figure S7). For ZnO, no bands belonging to O-H vibrations could be observed. The band at 3610 cm^{-1} can be assigned to the Brønsted acid sites [Si-(OH)-Al], while the band at 3740 cm^{-1} is related to the isolated silanols [Si-OH], typically located at the external surface.[18b] The shoulder band located at 3666 cm^{-1} can be assigned to the extra-framework aluminum species.[32] For the Zn-containing H-ZSM-5 samples, a new absorption band at 3715 cm^{-1} was observed, which can be assigned to the stretching O-H vibration of $[ZnOH]^+$ species.[33] The neutralization of BAS acidity by zinc migration was also quantitatively revealed by NH_3-TPD that both heat treatment and reaction promoted the migration of zinc to H-ZSM-5 (Figure 5c).

The Migration of Chromium and Zirconium

Different from In-based and Zn-based bifunctional catalysts, no visible element migration between oxides and H-ZSM-5 after CO_2 hydrogenation was observed by HAADF-STEM imaging over Cr-based and Zr-based bifunctional catalysts (Figures S8 and S9). Besides, the porosity and crystallinity of these two bifunctional catalysts after reaction were sustained (Figure S3). The spectroscopic characterizations confirmed that the chemical state of Cr_2O_3 and ZrO_2, and the acidity of H-ZSM-5 did not change significantly (Figure 6). All of these proofs suggested the physicochemical properties of each functional component were still kept even after reaction. The only observable change was the appearance of small border peaks (589.1 eV and 579.2 eV) and the slight loss of BAS acidity over Cr_2O_3/H-ZSM-5-*U* driven by reaction (Figure 6a–c), inferring that the reductive reaction condition could promote the migration of chromium species.

It was previously reported that the solid ion-exchange between Cr_2O_3 and H-ZSM-5 hardly took place even though the calcination temperature was above 800 °C.[34] This may be due to the low mobility of chromium ions in the Cr_2O_3 lattice (melting point 2260 °C). Cr_2O_3 can be reduced to low-valent $Cr^{\delta+}$ species ($\delta < 3$) below 350 °C (Figure S4). Therefore, the slight neutralization of BAS over Cr_2O_3/H-ZSM-5-*U* could be ascribed to the fact that Cr_2O_3 was partially reduced to the migratable low-valent $Cr^{\delta+}$ species in CO_2 hydrogenation. Due to the inert nature of ZrO_2, we did not observe any changes over the ZrO_2/H-ZSM-5 catalyst, no matter what kind of treatment the catalyst has suffered.

The Mechanism and Impact of Migration

The roles of zeolite, metal oxides, and the integration manners have been intensively illustrated in the bifunctional oxide-zeolite systems. However, the effect of metal migration to zeolite on the catalytic behaviors of CO/CO_2 conversion was often underestimated because it often causes irreversible deactivation. The investigation of metal migration not only

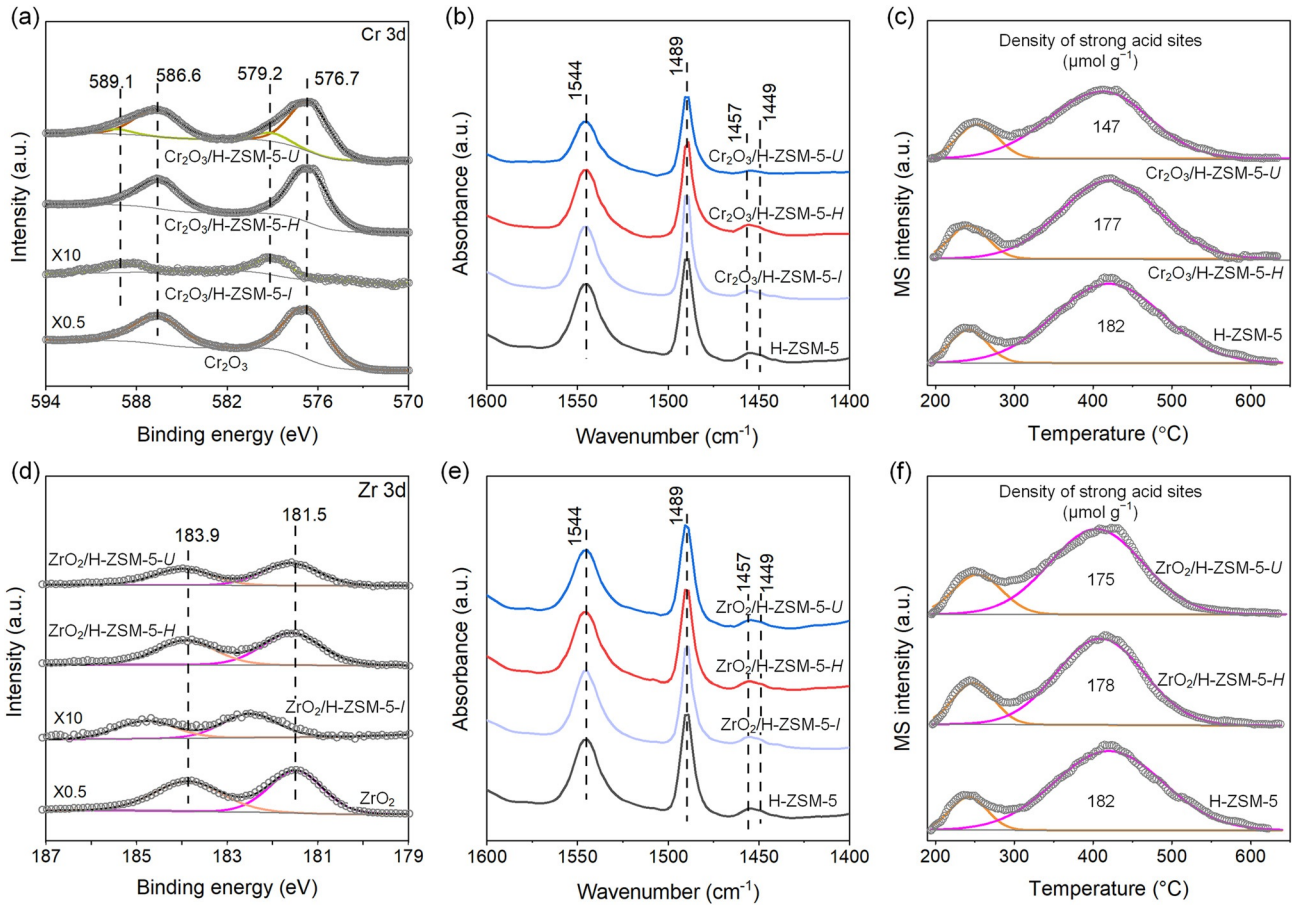

Figure 6. The spectra of a),d) XPS, b),e) pyridine-adsorption FTIR and c),f). NH_3-TPD profiles for H-ZSM-5, oxides and bifunctional catalysts prepared by different methods or treated by different condition (See details in the Supporting Information).

helps us to establish the relation between structure evolution and catalytic performance but also benefits the design of stable catalysts.

To confirm the location of migratable species, we measured the micropore volume of heat-treated and used bifunctional catalysts (Figure S10 and Table S3). For In_2O_3/H-ZSM-5-*H* and ZnO/H-ZSM-5-*H*, the micropore volume decreased compared with pristine H-ZSM-5, suggesting a fraction of micropore volume was filled by the metal species. Notably, the micropore volume of In_2O_3/H-ZSM-5-*U* further deceased after reaction, ascribing to the blockage of the micropores. For Cr_2O_3/H-ZSM-5 and ZrO_2/H-ZSM-5, however, the heat treatment and CO_2 hydrogenation reaction did not change the porosity of H-ZSM-5. The O_2-TPO was also performed to evaluate the effect of carbon deposition on the porosity of used catalysts (Figure S11). The peak areas for CO_2 formation originated from the combustion of carbon deposition decreased in the order of Cr_2O_3/H-ZSM-5 > In_2O_3/H-ZSM-5 > ZrO_2/H-ZSM-5 > ZnO/H-ZSM-5. However, the micropore volumes for the used catalysts decreased in the order of ZrO_2/H-ZSM-5 ≈ Cr_2O_3/H-ZSM-5 > ZnO/H-ZSM-5 > In_2O_3/H-ZSM-5 (Table S3). Therefore, it seems that carbon deposition is not the dominant factor that affecting the micropore volume of catalysts after reaction.

Thermal decomposition under argon confirmed that the In_2O_3 could be auto-reduced from 300 °C (Figure S12), which would result in the formation of monovalent In^+ ions ($In_2O_3 \rightarrow In_2O + O_2$).[27] The In^+ ions could incorporate into the zeolitic component and neutralize the protonic sites of zeolites.[27,35] We found that the activity of In_2O_3/H-ZSM-5 in the MTH reaction was much lower than that of H-ZSM-5 (Table S4), in line with the loss of BAS density driven by heat treatment (Figure 3c). Moreover, the neutralization of BAS and loss of zeolite crystallinity was probably accelerated by the reductive atmosphere or formed water vapor in CO_2 hydrogenation, because only traces of BAS survived after reaction (Figure 3b,c). As a result, almost no C_{2+} hydrocarbons were detected over In_2O_3/H-ZSM-5 (Figure 1a). Weber et al. also observed that a close distance between Na-promoted iron and H-ZSM-5 facilitated the migration of sodium ions from iron to H-ZSM-5, neutralizing the BAS.[11b] As summarized in Scheme 2a, the migration of indium to H-ZSM-5 could be driven by both heat treatment and reaction.

Likewise, our characterizations suggested that a proportion of protonic sites of H-ZSM-5 were possibly occupied by $[ZnOH]^+$ driven by heat treatment or reaction (Scheme 2b). The decrease of BAS density led to incomplete conversion of methanol and DME intermediates in CO_2 hydrogenation (Figure 1b). Meanwhile, the generation of CO from the

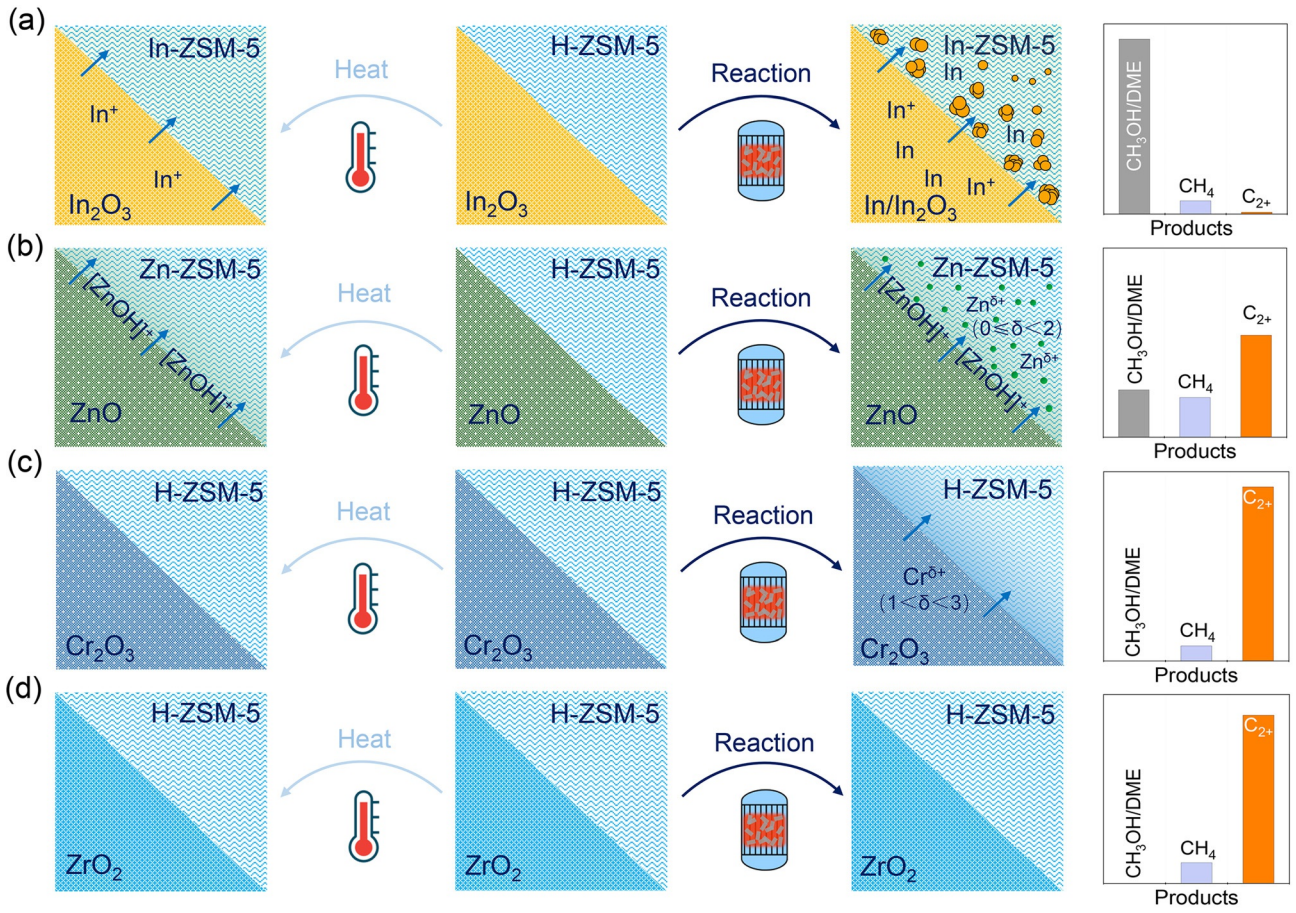

Scheme 2. Scheme of the element migration from oxide to H-ZSM-5 driven by heat treatment and CO_2 hydrogenation, and its impact on catalysis. a) In_2O_3/H-ZSM-5, b) ZnO/H-ZSM-5, c) Cr_2O_3/H-ZSM-5 and d) ZrO_2/H-ZSM-5.

RWGS reaction was faster over ZnO/H-ZSM-5 than that over ZnO ‖ H-ZSM-5 (Table S1). This could be attributed to the highly dispersed $[ZnOH]^+$ species, which were considered as the active sites for the RWGS reaction.[36] It is noteworthy that the low alkanes were the main products in CO_2 hydrogenation over ZnO/H-ZSM-5 (Table S1), while, the C_{5+} hydrocarbons selectivity exceeded 60% in methanol conversion over the same composite catalyst (Table S4). This might be due to the mechanism that the $[ZnOH]^+$ sites facilitated the hydrogenation of C_2–C_4 olefins and terminated the olefin oligomerization in the reaction atmosphere containing H_2.[18a,37]

Notably, a significant amount of indium NPs and zinc clusters were formed on the H-ZSM-5 (Scheme 2a,b), and this phenomenon could be attributed to two aspects. On the one hand, In_2O_3 could be reduced to its metallic liquid phase during the reaction, which could migrate and agglomerate to the surface of H-ZSM-5 crystals, leading to the formation of the indium NPs. Similarly, ZnO could also be reduced to its state of lower valence and became migratable species under reductive reaction conditions.[38] On the other hand, the harsh reaction conditions including exothermic nature, redox process, and the formation of water vapor might force the migratable In^+ and $[ZnOH]^+$ species to reassemble and form the clusters and nanoparticles. It is interesting that by varying the density of BAS of H-ZSM-5 (by changing Si/Al ratios), a higher proportion of acid sites was neutralized over H-ZSM-5-based bifunctional catalysts with a high density of BAS than those with a low density of BAS. This indicates that the migration of metal species to zeolites is probably bridged by the protonic [Si-OH-Al] sites on the zeolite surface because the low density of BAS means a long distance between two adjacent protonic sites (Figure S13).

Although the ion exchange hardly occurred during heat treatment over Cr_2O_3/H-ZSM-5, the ion migration did proceed in the stage of CO_2 hydrogenation (Scheme 2c). The accurate valence of chromium species after reaction was difficult to measure, but the Cr_2O_3 can be partially reduced below 350 °C (Figure S4). Since the monovalent species should be quite migratable over protonic sites, the valence of chromium species in bifunctional catalysts in CO_2 hydrogenation should be higher than 1 ($1 < \delta < 3$). The impact of ion migration for Cr_2O_3/H-ZSM-5 on CO_2 hydrogenation was weaker than that for In_2O_3/H-ZSM-5 and ZnO/H-ZSM-5. At least, all the methanol intermediates were completely converted into hydrocarbons. Over Cr_2O_3/H-ZSM-5, the C_{5+} selectivity could reach 63%, which was much higher than that (22%) of Cr_2O_3 ‖ H-ZSM-5 with the dual-bed configuration (Table S1). This indicates that the fabrication of H-ZSM-5 with a certain amount of chromium was beneficial to

the formation of long-chain hydrocarbons. The interaction between ZrO_2 and H-ZSM-5 was ignorable (Scheme 2d) due to the inert nature of ZrO_2. However, the ZrO_2 offered very low activity in CO_2 hydrogenation. It seems that the hydrogenation activity of oxides is related to their reducibility, and the reducibility decides the mobility of metal oxides in zeolites.

Considering the synergy between oxide and zeolite, the methanol intermediates formed on the oxide component should diffuse to zeolite for further conversion as fast as possible, as a result, intimate contact should be preferential. However, many reported cases demonstrated that close intimacy was detrimental for bifunctional catalysts, and an appropriate distance between two functional sites was profitable.[3b,4a,15] Sometimes, this phenomenon was superficially attributed to the speculative proximity effect. However, this might be problematic because the negative effect of close contact is caused by the interaction between the two components, not the spatial distance. The direct effect of element migration on bifunctional systems is that the integration manners of two components should be varied, depending on the oxide type. For instance, the granule-stacking manner with several hundred micrometers between zeolite and mobile In_2O_3 has been frequently used in CO_2 hydrogenation, while the close contact with the H-ZSM-5 and In_2O_3 would lead to the low selectivity of C_{2+} hydrocarbons and high selectivity of methanol.[4a,15] For chemically stable oxides such as Zr- and Cr-based bifunctional catalysts, the integration manner with intimate contact is often found to be beneficial for catalytic performance.[19a,21b,39] The universality of metal migration on zeolites is that the monovalent species are more migratable than the species at the higher valence. No matter the type of monovalent species (In^+ or $[ZnOH]^+$) are, these species can remarkably neutralize the Brønsted acid sites of H-ZSM-5. Besides, the migration of metals over zeolites probably proceeds by the spontaneous dispersion on support surface driven by high temperature and reductive atmosphere. The mobile species can partially block the micropore channels of H-ZSM-5. The preliminary findings in this work demonstrate that element migration is an important consideration when designing composite catalysts. The migration nature of each metal would determine the integration manners of final bifunctional catalysts.

Conclusion

In summary, the catalytic behaviors of bifunctional oxide-zeolite catalysts for the hydrogenation of CO_2 were significantly influenced by the interaction of the two functional components, and the extent was dependent on the type of oxides. The oxide components or their reduced species could migrate to zeolite surfaces and even into the micropore channels driven by harsh reaction conditions. The close contact between In_2O_3 or ZnO and zeolite would induce severe redistribution of metals and neutralization of BAS, destroying the bifunctionality. It is noteworthy that in some cases, the element migration would promote the reaction process towards the desired product, such as the formation of C_{5+} hydrocarbons over Cr_2O_3/H-ZSM-5. The oxide function employed in this work is unitary oxide, while the migration of metals in the frequently used binary or ternary oxides over zeolites may have different behaviors. The consequence of element migration, especially the neutralization of BAS, is often irreversible. Thus, the replacement of mobile elements, spatial separation of two functional sites, or immobilization of active elements by compounding can be considered to stabilize the performance of bifunctional catalysts. Our findings in this work would enrich the mechanistic understanding of the emerging bifunctional oxide-zeolite catalysts for C1 chemistry and provide insights into the rational design of bifunctional catalysts with an optimum composition and spatial organization.

Acknowledgements

This work was supported by the National Key Research and Development Program of Ministry of Science and Technology (No. 2019YFE0104400), the National Natural Science Foundation of China (Nos. 91945301, 22072120, 22002125, 21972116), the China Postdoctoral Science Foundation (Nos. 2019M662231, 2019TQ0178).

Conflict of Interest

The authors declare no conflict of interest.

Keywords: bifunctional catalysis · catalyst deactivation · CO_2 utilization · heterogeneous catalysis · zeolites

[1] a) Y. T. Cheng, J. Jae, J. Shi, W. Fan, G. W. Huber, *Angew. Chem. Int. Ed.* **2012**, *51*, 1387–1390; *Angew. Chem.* **2012**, *124*, 1416–1419; b) Z. Guo, X. Li, S. Hu, G. Ye, X. Zhou, M. O. Coppens, *Angew. Chem. Int. Ed.* **2020**, *59*, 1548–1551; *Angew. Chem.* **2020**, *132*, 1564–1567; c) W. Zhou, K. Cheng, J. Kang, C. Zhou, V. Subramanian, Q. Zhang, Y. Wang, *Chem. Soc. Rev.* **2019**, *48*, 3193–3228.

[2] a) Y. Liu, D. Deng, X. Bao, *Chem* **2020**, *6*, 2497–2514; b) M. Andersen, A. J. Medford, J. K. Norskov, K. Reuter, *Angew. Chem. Int. Ed.* **2016**, *55*, 5210–5214; *Angew. Chem.* **2016**, *128*, 5296–5300; c) J. Bao, G. Yang, Y. Yoneyama, N. Tsubaki, *ACS Catal.* **2019**, *9*, 3026–3053.

[3] a) F. Jiao, J. Li, X. Pan, J. Xiao, H. Li, H. Ma, M. Wei, Y. Pan, Z. Zhou, M. Li, S. Miao, J. Li, Y. Zhu, D. Xiao, T. He, J. Yang, F. Qi, Q. Fu, X. Bao, *Science* **2016**, *351*, 1065–1068; b) K. Cheng, B. Gu, X. Liu, J. Kang, Q. Zhang, Y. Wang, *Angew. Chem. Int. Ed.* **2016**, *55*, 4725–4728; *Angew. Chem.* **2016**, *128*, 4803–4806; c) Z. Li, J. Wang, Y. Qu, H. Liu, C. Tang, S. Miao, Z. Feng, H. An, C. Li, *ACS Catal.* **2017**, *7*, 8544–8548.

[4] a) P. Gao, S. Li, X. Bu, S. Dang, Z. Liu, H. Wang, L. Zhong, M. Qiu, C. Yang, J. Cai, W. Wei, Y. Sun, *Nat. Chem.* **2017**, *9*, 1019–1024; b) K. Cheng, W. Zhou, J. Kang, S. He, S. Shi, Q. Zhang, Y. Pan, W. Wen, Y. Wang, *Chem* **2017**, *3*, 334–347; c) Y. Ni, Z. Chen, Y. Fu, Y. Liu, W. Zhu, Z. Liu, *Nat. Commun.* **2018**, *9*, 3457; d) Z. Li, Y. Qu, J. Wang, H. Liu, M. Li, S. Miao, C. Li, *Joule* **2019**, *3*, 570–583.

[5] a) Q. Zhang, J. Yu, A. Corma, *Adv. Mater.* **2020**, *32*, 2002927; b) N. Li, F. Jiao, X. Pan, Y. Chen, J. Feng, G. Li, X. Bao, *Angew. Chem. Int. Ed.* **2019**, *58*, 7400–7404; *Angew. Chem.* **2019**, *131*,

7478 – 7482; c) A. Dokania, A. Ramirez, A. Bavykina, J. Gascon, *ACS Energy Lett.* **2019**, *4*, 167 – 176.
[6] X. Liu, M. Wang, C. Zhou, W. Zhou, K. Cheng, J. Kang, Q. Zhang, W. Deng, Y. Wang, *Chem. Commun.* **2018**, *54*, 140 – 143.
[7] C. H. Bartholomew, *Appl. Catal. A* **2001**, *212*, 17 – 60.
[8] a) S. S. Arora, D. L. S. Nieskens, A. Malek, A. Bhan, *Nat. Catal.* **2018**, *1*, 666 – 672; b) X. Zhao, J. Li, P. Tian, L. Wang, X. Li, S. Lin, X. Guo, Z. Liu, *ACS Catal.* **2019**, *9*, 3017 – 3025; c) M. Wang, Z. Wang, S. Liu, R. Gao, K. Cheng, L. Zhang, G. Zhang, X. Min, J. Kang, Q. Zhang, Y. Wang, *J. Catal.* **2021**, *394*, 181 – 192.
[9] a) D. Miao, Y. Ding, T. Yu, J. Li, X. Pan, X. Bao, *ACS Catal.* **2020**, *10*, 7389 – 7397; b) J. Zhang, M. Zhang, S. Chen, X. Wang, Z. Zhou, Y. Wu, T. Zhang, G. Yang, Y. Han, Y. Tan, *Chem. Commun.* **2019**, *55*, 973 – 976.
[10] a) J. Lu, B. Fu, M. C. Kung, G. Xiao, J. W. Elam, H. H. Kung, P. C. Stair, *Science* **2012**, *335*, 1205 – 1208; b) M. Ye, H. Li, Y. Zhao, T. Zhang, Z. Liu, *Adv. Chem. Eng.* **2015**, *47*, 279 – 335; c) L. Liu, A. Corma, *Nat. Rev. Chem.* **2021**, *5*, 256 – 276.
[11] a) F. G. Botes, W. Böhringer, *Appl. Catal. A* **2004**, *267*, 217 – 225; b) J. L. Weber, N. A. Krans, J. P. Hofmann, E. J. M. Hensen, J. Zecevic, P. E. de Jongh, K. P. de Jong, *Catal. Today* **2020**, *342*, 161 – 166; c) C. W. Andersen, E. Borfecchia, M. Bremholm, M. R. V. Jorgensen, P. N. R. Vennestrom, C. Lamberti, L. F. Lundegaard, B. B. Iversen, *Angew. Chem. Int. Ed.* **2017**, *56*, 10367 – 10372; *Angew. Chem.* **2017**, *129*, 10503 – 10508.
[12] H. G. Karge, H. K. Beyer, *Stud. Surf. Sci. Catal.* **1991**, *69*, 43 – 64.
[13] a) H. G. Karge, *Stud. Surf. Sci. Catal.* **1997**, *105*, 1901 – 1948; b) A. V. Kucherov, A. A. Slinkin, *J. Mol. Catal.* **1994**, *90*, 323 – 354.
[14] Y. C. Xie, Y. Q. Tang, *Adv. Catal.* **1990**, *37*, 1 – 43.
[15] P. Gao, S. Dang, S. Li, X. Bu, Z. Liu, M. Qiu, C. Yang, H. Wang, L. Zhong, Y. Han, Q. Liu, W. Wei, Y. Sun, *ACS Catal.* **2018**, *8*, 571 – 578.
[16] a) M. Shamzhy, M. Opanasenko, P. Concepción, A. Martínez, *Chem. Soc. Rev.* **2019**, *48*, 1095 – 1149; b) D. Ma, W. Zhang, Y. Shu, X. Liu, Y. Xu, X. Bao, *Catal. Lett.* **2000**, *66*, 155 – 160.
[17] D. Ma, X. Han, D. Zhou, Z. Yan, R. Fu, Y. Xu, X. Bao, H. Hu, S. C. F. Au-Yeung, *Chem. Eur. J.* **2002**, *8*, 4557 – 4561.
[18] a) X. Niu, J. Gao, Q. Miao, M. Dong, G. Wang, W. Fan, Z. Qin, J. Wang, *Microporous Mesoporous Mater.* **2014**, *197*, 252 – 261; b) I. Pinilla-Herrero, E. Borfecchia, J. Holzinger, U. V. Mentzel, F. Joensen, K. A. Lomachenko, S. Bordiga, C. Lamberti, G. Berlier, U. Olsbye, S. Svelle, J. Skibsted, P. Beato, *J. Catal.* **2018**, *362*, 146 – 163.
[19] a) Y. Wang, L. Tan, M. Tan, P. Zhang, Y. Fang, Y. Yoneyama, G. Yang, N. Tsubaki, *ACS Catal.* **2019**, *9*, 895 – 901; b) C. Zhou, J. Shi, W. Zhou, K. Cheng, Q. Zhang, J. Kang, Y. Wang, *ACS Catal.* **2020**, *10*, 302 – 310; c) O. Martin, A. J. Martín, C. Mondelli, S. Mitchell, T. F. Segawa, R. Hauert, C. Drouilly, D. Curulla-Ferré, J. Pérez-Ramírez, *Angew. Chem. Int. Ed.* **2016**, *55*, 6261 – 6265; *Angew. Chem.* **2016**, *128*, 6369 – 6373.
[20] a) K. Cheng, J. Kang, D. L. King, V. Subramanian, C. Zhou, Q. Zhang, Y. Wang, *Adv. Catal.* **2017**, *60*, 125 – 208; b) X. Pan, F. Jiao, D. Miao, X. Bao, *Chem. Rev.* **2021**, *121*, 6588 – 6609.
[21] a) Z. Ma, M. D. Porosoff, *ACS Catal.* **2019**, *9*, 2639 – 2656; b) S. Wang, L. Zhang, W. Zhang, P. Wang, Z. Qin, W. Yan, M. Dong, J. Li, J. Wang, L. He, U. Olsbye, W. Fan, *Chem* **2020**, *6*, 3344 – 3363; c) M. T. Arslan, B. Ali, S. Z. A. Gilani, Y. Hou, Q. Wang, D. Cai, Y. Wang, F. Wei, *ACS Catal.* **2020**, *10*, 2477 – 2488.
[22] L. Tan, F. Wang, P. Zhang, Y. Suzuki, Y. Wu, J. Chen, G. Yang, N. Tsubaki, *Chem. Sci.* **2020**, *11*, 4097 – 4105.
[23] a) W. Dai, X. Wang, G. Wu, N. Guan, M. Hunger, L. Li, *ACS Catal.* **2011**, *1*, 292 – 299; b) U. Olsbye, S. Svelle, K. P. Lillerud, Z. H. Wei, Y. Y. Chen, J. F. Li, J. G. Wang, W. B. Fan, *Chem. Soc. Rev.* **2015**, *44*, 7155 – 7176.
[24] H. Xiao, J. Zhang, X. Wang, Q. Zhang, H. Xie, Y. Han, Y. Tan, *Catal. Sci. Technol.* **2015**, *5*, 4081 – 4090.
[25] S. Zheng, H. R. Heydenrych, A. Jentys, J. A. Lercher, *J. Phys. Chem. B* **2002**, *106*, 9552 – 9558.
[26] K. Cheng, J. Kang, S. Huang, Z. You, Q. Zhang, J. Ding, W. Hua, Y. Lou, W. Deng, Y. Wang, *ACS Catal.* **2012**, *2*, 441 – 449.
[27] M. R. Mihályi, H. K. Beyer, *Chem. Commun.* **2001**, 2242 – 2243.
[28] C. V. Hidalgo, H. Itoh, T. Hattori, M. Niwa, Y. Murakami, *J. Catal.* **1984**, *85*, 362 – 369.
[29] L. J. Lobree, I.-C. Hwang, J. A. Reimer, A. T. Bell, *J. Catal.* **1999**, *186*, 242 – 253.
[30] N. Katada, H. Igi, J.-H. Kim, *J. Phys. Chem. B* **1997**, *101*, 5969 – 5977.
[31] P. Tynjälä, T. T. Pakkanen, *J. Mol. Catal. A* **1996**, *110*, 153 – 161.
[32] M. B. Sayed, R. A. Kydd, R. P. Cooney, *J. Catal.* **1984**, *88*, 137 – 149.
[33] K. Wang, G. Cao, G. J. Kennedy, M. Afeworki, R. E. Bare, R. B. Hall, *J. Phys. Chem. C* **2011**, *115*, 18611 – 18617.
[34] A. V. Kucherov, A. A. Slinkin, *Zeolites* **1987**, *7*, 38 – 42.
[35] R. M. Mihályi, Z. Schay, Á. Szegedi, *Catal. Today* **2009**, *143*, 253 – 260.
[36] Z. Zhang, H. Yin, G. Yu, S. He, J. Kang, Z. Liu, K. Cheng, Q. Zhang, Y. Wang, *J. Catal.* **2021**, *395*, 350 – 361.
[37] Y. Chen, K. Gong, F. Jiao, X. Pan, G. Hou, R. Si, X. Bao, *Angew. Chem. Int. Ed.* **2020**, *59*, 6529 – 6534; *Angew. Chem.* **2020**, *132*, 6591 – 6596.
[38] a) A. Seidel, F. Rittner, B. Boddenberg, *J. Chem. Soc. Faraday Trans.* **1996**, *92*, 493 – 497; b) F. Rittner, A. Seidel, B. Boddenberg, *Microporous Mesoporous Mater.* **1998**, *24*, 127 – 131; c) M. Behrens, F. Studt, I. Kasatkin, S. Kühl, M. Hävecker, F. Abild-Pedersen, S. Zander, F. Girgsdies, P. Kurr, B.-L. Kniep, M. Tovar, R. W. Fischer, J. K. Nørskov, R. Schlögl, *Science* **2012**, *336*, 893; d) T. Lunkenbein, J. Schumann, M. Behrens, R. Schlögl, M. G. Willinger, *Angew. Chem. Int. Ed.* **2015**, *54*, 4544 – 4548; *Angew. Chem.* **2015**, *127*, 4627 – 4631.
[39] X. Liu, W. Zhou, Y. Yang, K. Cheng, J. Kang, L. Zhang, G. Zhang, X. Min, Q. Zhang, Y. Wang, *Chem. Sci.* **2018**, *9*, 4708 – 4718.

Manuscript received: May 31, 2021
Accepted manuscript online: June 8, 2021
Version of record online: June 30, 2021

